AGU PUBLICATIONS

JGR

Journal of Geophysical Research: Atmospheres

RESEARCH ARTICLE
10.1002/2016JD025410

Key Points:
- Reanalyses can reproduce seasonal cycle and interannual variability of land surface temperature (LST)
- Trends in reanalysis LST were underestimated over ~70% of global deserts
- Stronger warming amplification in deserts was observed than in semiarid regions

Supporting Information:
- Supporting Information S1

Correspondence to:
K. Wang,
kcwang@bnu.edu.cn

Citation:
Zhou, C., and K. Wang (2016), Land surface temperature over global deserts: Means, variability, and trends, *J. Geophys. Res. Atmos.*, *121*, doi:10.1002/2016JD025410.

Received 24 MAY 2016
Accepted 26 NOV 2016
Accepted article online 6 DEC 2016

Land surface temperature over global deserts: Means, variability, and trends

Chunlüe Zhou[1,2] **and Kaicun Wang**[1,2]

[1]College of Global Change and Earth System Science, Beijing Normal University, Beijing, China, [2]Joint Center for Global Change Studies, Beijing, China

Abstract Land surface air temperature (LSAT) has been a widely used metric to study climate change. Weather observations of LSAT are the fundamental data for climate change studies and provide key evidence of global warming. However, there are very few meteorological observations over deserts due to their uninhabitable environment. This study fills this gap and provides independent evidence using satellite-derived land surface temperatures (LSTs), benefiting from their global coverage. The frequency of clear sky from MODerate Resolution Imaging Spectroradiometer (MODIS) LST data over global deserts was found to be greater than 94% for the 2002–2015 period. Our results show that MODIS LST has a bias of 1.36°C compared to ground-based observations collected at 31 U.S. Climate Reference Network (USCRN) stations, with a standard deviation of 1.83°C. After bias correction, MODIS LST was used to evaluate existing reanalyses, including ERA-Interim, Japanese 55-year Reanalysis (JRA-55), Modern-Era Retrospective Analysis for Research and Applications (MERRA), MERRA-land, National Centers for Environmental Prediction (NCEP)-R1, and NCEP-R2. The reanalyses accurately reproduce the seasonal cycle and interannual variability of the LSTs, but their multiyear means and trends of LSTs exhibit large uncertainties. The multiyear averaged LST over global deserts is 23.5°C from MODIS and varies from 20.8°C to 24.5°C in different reanalyses. The MODIS LST over global deserts increased by 0.25°C/decade from 2002 to 2015, whereas the reanalyses estimated a trend varying from −0.14 to 0.10°C/decade. The underestimation of the LST trend by the reanalyses occurs for approximately 70% of the global deserts, likely due to the imperfect performance of the reanalyses in reproducing natural climate variability.

1. Introduction

Global deserts occupy approximately one quarter of the Earth's land surface [*Ezcurra*, 2006]. This ratio of deserts to global land area has been projected to increase with global warming [*Huang et al.,* 2015]. Desertification in the semiarid regions in the past several decades has contributed a negative forcing by reflecting more solar radiation, equivalent to ~20% of the global anthropogenic CO_2 effect [*Rotenberg and Yakir*, 2010].

Weather observations of land surface air temperature (LSAT) have been the essential data for studies of climate change and provide key evidence for global warming. However, there are very few weather stations in deserts because of their uninhabitable environment. This issue is well recognized (i.e., by *Intergovernmental Panel on Climate Change* (*IPCC*) [2013] reports) but has not been resolved. For example, the recent warming slowdown has been questioned owing to insufficient temperature data coverage [*Cowtan and Way*, 2014; *Karl et al.,* 2015]. In spite of the wide usage of current temperature data sets from the Hadley Centre-Climatic Research Unit [*Harris et al.,* 2014], the Goddard Institute for Space Studies [*Hansen et al.,* 1999], the Global Historical Climatology Network Monthly [*Lawrimore et al.,* 2011], and others, they do not completely cover high latitudes and global deserts, where in situ measurements are very scarce and expensive.

Arid regions around the world are often considered particularly sensitive to climatic change. *Lim et al.* [2005] and *Zhou et al.* [2015] found that the warming rate over drylands is greater than over the rest and is even stronger in winter [*Huang et al.,* 2012]. The warming trend of daily minimum temperature and the decreasing trend of diurnal temperature range are stronger in drier regions [*Zhou et al.,* 2007, 2009, 2010]. There is a general agreement among most models that warming of over 3°C is expected for drylands by the end of the 21st century [*IPCC*, 2013]. During the period 1973 to 2014, relative humidity has been decreasing [*Blunden and Arndt*, 2015]. However, these conclusions may need to be revaluated

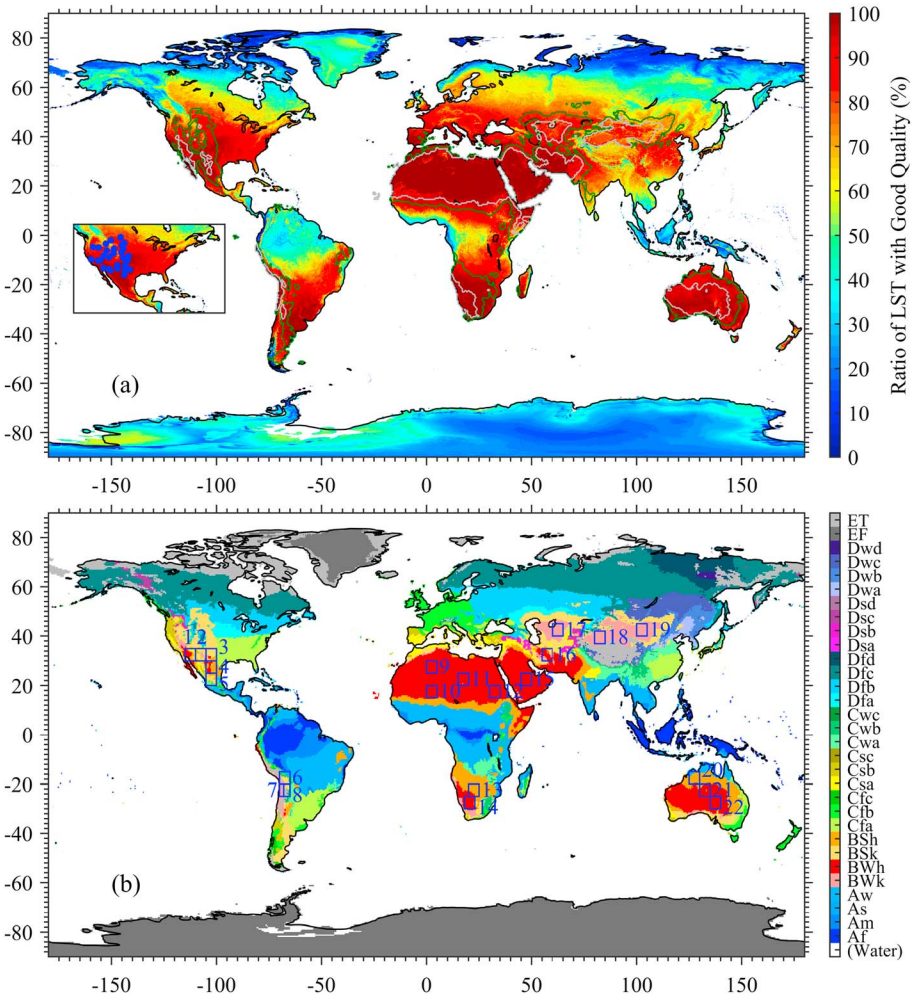

Figure 1. (a) Good data availability of MODIS satellite-derived land surface temperatures (LSTs) from August 2002 to August 2015 (Unit: %). (b) Köppen-Geiger climate classifications were used to identify deserts. The MODIS LST data availability is 94.5% ± 8.18% over deserts and 89.24% ± 9.48% over semiarid regions. LSTs collected at 31 U.S. Climate Reference Network (USCRN) sites (blue dots inside the top figure) were used to evaluate and correct the MODIS LST data. We selected 22 subregions of 5° × 5° (except for A7 of 2° × 5° in Chile) to study the LST variability and its determining factors.

because of the data used, which are not from the observation data or are based on incomplete global sampling of LSAT.

Satellite data with global coverage have become available. Previous study has investigated global and regional trends in land surface temperature (LST) using 2000–2011 data [*Sobrino and Julien*, 2013]. Here we found that the availability of LST is up to 94.45% (±8.18% STD) over arid/desert regions and 89.24% (±9.48% STD) over semiarid regions (Figure 1), without changing over the time (Figure S1 in the supporting information), for MODerate Resolution Imaging Spectroradiometer (MODIS) data from the National Aeronautics and Space Administration (NASA) Earth observation system Terra (overpass times at 10:30 and 22:30 local time) and Aqua (overpass times at 13:30 and 1:30 local time) polar-orbiting satellite platforms. Moreover, far fewer human disturbances of land cover and land use are present in desert areas, making it easier to attribute the observed climate changes to anthropogenic greenhouse effects and natural climate variability.

In this study, we first utilized 5 min LST measurements at 31 arid/desert and semiarid stations from the U.S. Climate Reference Network (USCRN) to compare the LST data derived from MODIS and found that the MODIS LSTs closely match the in situ observed LSTs. We selected arid/desert (semiarid) regions as referenced

regions due to their extremely low cloud frequency and fraction, i.e., the data availability of MODIS LST being higher than 94% (Figures 1 and S1). Then we examined and analyzed the mean state, variability, and trend of LSTs in the currently available reanalyses, including ERA-Interim, Japanese 55 year Reanalysis (JRA-55), Modern-Era Retrospective Analysis for Research and Applications (MERRA), MERRA-land, National Centers for Environmental Prediction Reanalysis 1 (NCEP-R1), and NCEP-R2. We found that the seasonal cycle and interannual variability of LSTs can be reproduced by the reanalyses, but the multiyear mean and trend of LST in the reanalyses have large uncertainties. The MODIS LST trend averaged over global deserts (0.25°C/decade) is far larger than that of the reanalyses (−0.14 to 0.10°C/decade) for the 2002–2015 period. This underestimation of the LST trend by the reanalyses can be detected for approximately 70% of the global deserts. Furthermore, our results confirm the higher warming rate in arid areas (deserts) than in semiarid areas.

2. Study Region and Data Set Description

2.1. Arid/Desert and Semiarid Regions

We selected the Köppen climate classification based on climatological temperatures and precipitation [*Kottek et al.,* 2006] to identify deserts at 0.5° × 0.5° grids. To determine whether arid areas (deserts) have a higher warming rate than semiarid areas [*Huang et al.,* 2012; *Lim et al.,* 2005; *Zhou et al.,* 2015], we also compared LST trends over arid and semiarid regions. The Köppen climate classification treats semiarid (or steppe) climates (BSk and BSh) as intermediates between arid/desert climates (BWk and BWh) and humid climates in terms of ecological characteristics and agricultural potential (Figure 1). Arid/desert regions mainly include barren land, whereas semiarid areas are usually dominated by either grasses or shrubs.

2.2. Satellite-Derived Land Surface Temperatures

LSTs derived from MODIS including MOD11C3 and MYD11C3 were used in this study. Two MODIS instruments [*Salomonson et al.,* 1989] were launched to study the atmosphere, land, and ocean on 18 December 1999, on a morning platform called Terra (overpass times at 10:30 and 22:30 local time, corresponding to MOD11C3) and on 4 May 2002, on an afternoon platform called Aqua (overpass times at 13:30 and 1:30 local time, corresponding to MYD11C3). In this study, we used MODIS monthly composited and averaged LST data at 0.05° × 0.05° spatial resolution, which are retrieved from a day/night algorithm [*Wan and Li*, 1997]. In the day/night algorithm, LSTs and emissivity are retrieved from pairs of day and night observations in seven middle and thermal infrared bands. MODIS LST products have been validated through a series of field campaigns that have demonstrated these products to be highly accurate, with an error of 1–2 K in most cases [*Coll et al.,* 2005, 2009; *Li et al.,* 2013a; *Tomlinson et al.,* 2011; *Wan and Li*, 2008; *Wan et al.,* 2002; *Wang and Liang*, 2009; *Wang et al.,* 2007]. Furthermore, MODIS LSTs were used to assess global or regional climate models [*Trigo et al.,* 2015; *Wang et al.,* 2014].

2.3. Ground-Based Land Surface Temperatures

Satellite-derived LST products were compared here with ground-based LST observations collected by the U.S. Climate Reference Network (USCRN). The USCRN is a systematic and sustained network of climate monitoring stations with 114 sites across the conterminous U.S., Alaska, and Hawaii [*Diamond et al.,* 2013]. These stations use high-quality instruments to measure temperature (including LST), precipitation, wind speed, soil conditions, and other variables, with triple redundancy for intercomparison and quality assurance [*Diamond et al.,* 2013; *Hubbard et al.,* 2005]. Therefore, the USCRN network was created to provide high-quality data for climate research, which has a strict requirement on its instruments and the located environment. These stations are placed in as open and homogeneous area as possible, such as conservation areas, national parks, grasslands, and wildlife refuges. More detailed photographs of all the stations are available on the USCRN website (http://www.ncdc.noaa.gov/crn/photos.html).

LST is precisely measured by Apogee's infrared radiometers pointed at the ground surface. These instruments convert thermal energy radiated from the surface to LST with default constant land surface emissivity, based on the Stefan-Boltzmann law [*Diamond et al.,* 2013; *Gallo et al.,* 2011]. The correction of downward longwave radiation should be considered [*Wang et al.,* 2014; *Zeng et al.,* 2012]. The 5 min LST measurements available for 2012 to 2015 from 31 sites in arid/desert and semiarid regions were used in this study (Figure 1). The elevations of 31 sites range from 24 m to 2017 m with an average of approximately 1169 m.

Table 1. Summative Information on Reanalyses[a]

Reanalysis	Institution	Model Resolution	Data Resolution	Period	Assimilation Systems
NCEP-R1	National Oceanic and Atmospheric Administration (NOAA) National Center for Environmental Prediction (NCEP)	T62 ~ 210 km	5/2° × 5/2°	1948 and afterward	3D-VAR
NCEP-R2	National Oceanic and Atmospheric Administration (NOAA) National Center for Environmental Prediction (NCEP)	T62 ~ 210 km	5/2° × 5/2°	1948 and afterward	3D-VAR
MERRA	National Aeronautics and Space Administration's Goddard Space Flight Center (NASA's GSFC) Global Modeling and Assimilation Office (GMAO)	1/2° × 2/3° ~55 km	1/2° × 2/3°	1979 and afterward	3D-VAR
MERRA-land	National Aeronautics and Space Administration's Goddard Space Flight Center (NASA's GSFC) Global Modeling and Assimilation Office (GMAO)	1/2° × 2/3° ~55 km	1/2° × 2/3°	1979 and afterward	4D-VAR
ERA-Interim	European Centre for Medium-Range Weather Forecasts (ECMWF)	T255 ~ 80 km	3/4° × 3/4°	1979 and afterward	4D-VAR
JRA-55	Japan Meteorological Agency	T319 ~ 55 km	5/4° × 5/4°	1958–2013	4D-VAR

[a]GSFC, Goddard Space Flight Center.

2.4. Reanalysis Land Surface Temperatures

Reanalysis data sets have been widely used in climate studies as important auxiliary observations [*Dee et al.,* 2014]. The performances of existing reanalyses, including ERA-Interim [*Dee et al.,* 2011b], JRA-55 [*Kobayashi et al.,* 2015], MERRA [*Rienecker et al.,* 2011], MERRA-land [*Reichle et al.,* 2011], NCEP-R1 [*Kalnay et al.,* 1996], and NCEP-R2 [*Kanamitsu et al.,* 2002], in simulating LST were evaluated in this study. MERRA, NCEP-R1, and NCEP-R2 adopt three-dimensional variational assimilation systems (3D-VAR), whereas ERA-Interim, JRA-55, and MERRA-land employ four-dimensional variational systems (4D-VAR). The reanalyses assimilate many of the basic upper air atmospheric fields including air temperature, surface pressure, satellite radiances, etc. from multiple sources; however, LSTs in the reanalyses are pure model calculations without assimilating LST observations for the lack for global observing network of LST [*Zhou and Wang*, 2016c]. The reanalysis LSTs are derived from the surface energy balance inside each tile, which links the surface with the lowest model level through dry static energy and moisture [*Best et al.,* 2004]. The MERRA-land LST is averaged from hourly outputs of offline Land Surface Model simulation forced by bias-corrected MERRA reanalysis, which is considered to be more accurate for land surface hydrological studies[*Reichle et al.,* 2011]. The information on horizontal and temporal resolution of reanalysis is listed in Table 1. More details on the reanalyses can be found in the supporting information [*Briegleb and Ramanathan*, 1982; *Chou and Lee*, 1996; *Hong and Pan*, 1996; *Kanamitsu et al.,* 2002].

The broadband emissivity is a key parameter in determining LST using the energy budget equation [*Wang et al.,* 2005]. In the window region (the 800–1250 cm^{-1} spectral region), the emissivity (ε) is set to be constant for open water, sea ice, exposed snow cover, the interception layer, and desert areas in ERA-Interim. For high- and low-vegetation areas, shaded snow, and bare ground, the ε depends on the land cover type and water content in the top soil layer. The ε decreases linearly from 0.96 for soils at or above field capacity to 0.93 for soils at or below permanent wilting point. Outside the 800–1250 cm^{-1} spectral region, ε is assumed to be a fixed value everywhere, for example, 0.99 in ERA-Interim. A similar formulation is used in the other reanalyses.

To compare reanalyzed LST with MODIS LST, as the ERA-Interim, we interpolate all the reanalyzed LST and MODIS LST into 1° × 1° grids with bilinear interpolation algorithm, i.e., a linear interpolation functions on two-dimensional grids. To assess the MODIS LST with USCRN LST, we bilinearly interpolate MODIS LST into site level at 31 stations in arid and semiarid regions.

2.5. Surface Ocean State and Atmosphere Teleconnection

To investigate the associated dynamic processes associated with LST and their relationship to the LST trends in the reanalyses, several interannual climate variabilities such as surface ocean indices over the Pacific, Atlantic, and Indian Oceans and sea ice changes were used here.

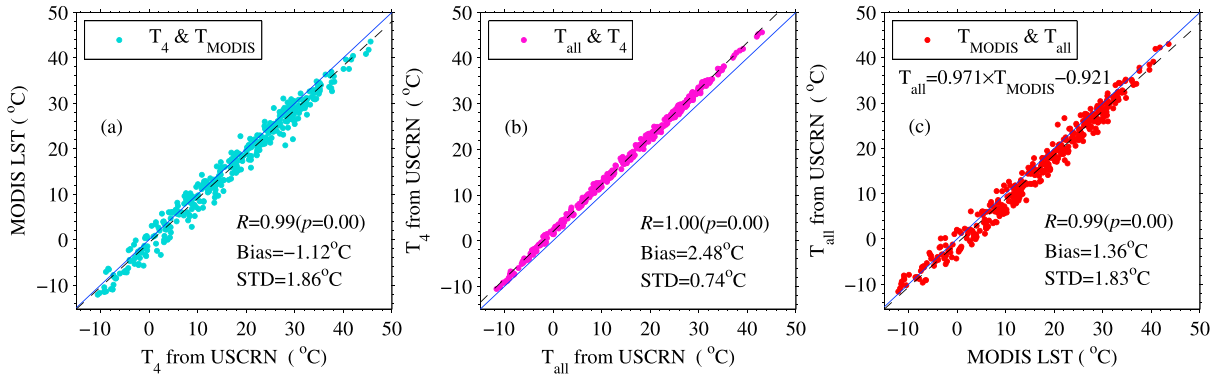

Figure 2. Comparisons of Moderate Resolution Imaging Spectroradiometer (MODIS) monthly land surface temperatures (LSTs) with the U.S. Climate Reference Network (USCRN) LSTs from February 2012 to September 2015 at 31 sites (as shown in Figure 1). T_{all} is the average of all LSTs measured at 5 min intervals at the USCRN stations. T_4 is the average of the four USCRN LSTs during the 5 min interval corresponding to the MODIS satellite overpass (i.e., 1:30, 10:30, 13:30, and 22:30 local time). T_{MODIS} refers to the mean LST averaged from these daily four MODIS LST retrievals. The statistical parameter correlation coefficient (R), bias, and standard deviation (STD) are also shown.

The surface ocean indices used in this study include the Niño1 + 2, Niño3, Niño4, and Niño3.4 anomalies and the Trans-Niño Index [*Trenberth and Stepaniak*, 2001] over the tropical Pacific Ocean; the Northern Oscillation Index [*Schwing et al.,* 2002], Tripole Index for Pacific Oscillation [*Henley et al.,* 2015], Western Hemisphere warm pool [*Wang and Enfield*, 2001] and Pacific/North American over the Pacific ocean [*Trenberth and Hurrell*, 1994]; and the Western Tropical Indian Ocean, Southeastern Tropical Indian Ocean, Indian Ocean Dipole, Southern Oscillation Index [*Trenberth*, 1984], and Quasi-Biennial Oscillation [*Baldwin et al.,* 2001] over the Indian Ocean. Some indices from the Atlantic Ocean including North Atlantic Tropical Index and Atlantic Meridional Mode-wind index, etc. were used [*Chang et al.,* 1997; *Chiang and Vimont*, 2004; *Enfield et al.,* 1999]. Northern Oscillation Indices including Polar/Eurasia Pattern, Pacific Transition Pattern, etc. reflect main patterns of atmospheric teleconnection [*Barnston and Livezey*, 1987; *Halpert and Bell*, 1997; *Wallace and Gutzler*, 1981]. The sea ice indices include the Sea Ice Extent Anomaly and Sea Ice Cover Anomaly over the Northern and Southern Hemispheres. More details can be found in the supporting information.

3. Results

3.1. Evaluation and Bias Correction of MODIS Land Surface Temperatures

In this section, we assessed the capability of MODIS LST in quantifying (1) instantaneous LST, (2) daily mean LST based on its four-time samples (T_4), and (3) LST under all conditions including clear- and cloudy-sky conditions based on MODIS daily mean LST. The third step is designed for the use of bias-corrected MODIS LST to evaluate reanalysis LST.

We first compared MODIS LST at 0.05° grids with ground-based observations of LST at 31 USCRN stations in arid/desert and semiarid regions to quantify its accuracy in reflecting instantaneous and daily LST (Figure 1). The analysis shows a nearly identical seasonal cycle ($R = 0.99$, $p = 0.00$) between monthly mean MODIS LST and USCRN LST for the four-satellite overpass times (T_4) and the average from continuous 5 min observations (T_{all}) (Figures 2a and 2c). When MODIS LST is compared with T_4 at four MODIS satellite overpass times, T_{MODIS} relative to T_4 has an error of −1.12°C (±1.86°C STD) (Figure 2a). This result is consistent with the comparison result of *Wang et al.* [2014] that MODIS LST has site-averaged −1.18°C (±3.94°C STD), recalculated from Table 2 in *Wang et al.* [2014] on the four satellite overpass times and then averaged into daily value of −1.18°C (±1.42°C STD) at four selected semiarid stations in July 2003.

To test whether the four MODIS samples can represent the daily mean of LST in the reanalyses that averaged from a model step (e.g., 30 min in ERA-Interim [*Dee et al.,* 2011b]), we compared the T_4 from four MODIS satellite overpass times with T_{all} at USCRN and found that the sample bias of T_4 relative to T_{all} is 2.48°C (±0.74°C STD) (Figure 2b). This sample bias tends to increase with temperature, exhibiting a departure from the 1:1 line (Figure 2b), which closely correlates with the partitioning of surface available energy between latent and sensible heat fluxes [*Wang*, 2014; *Wang and Zhou*, 2015; *Zhou and Wang,* 2016a, 2016c].

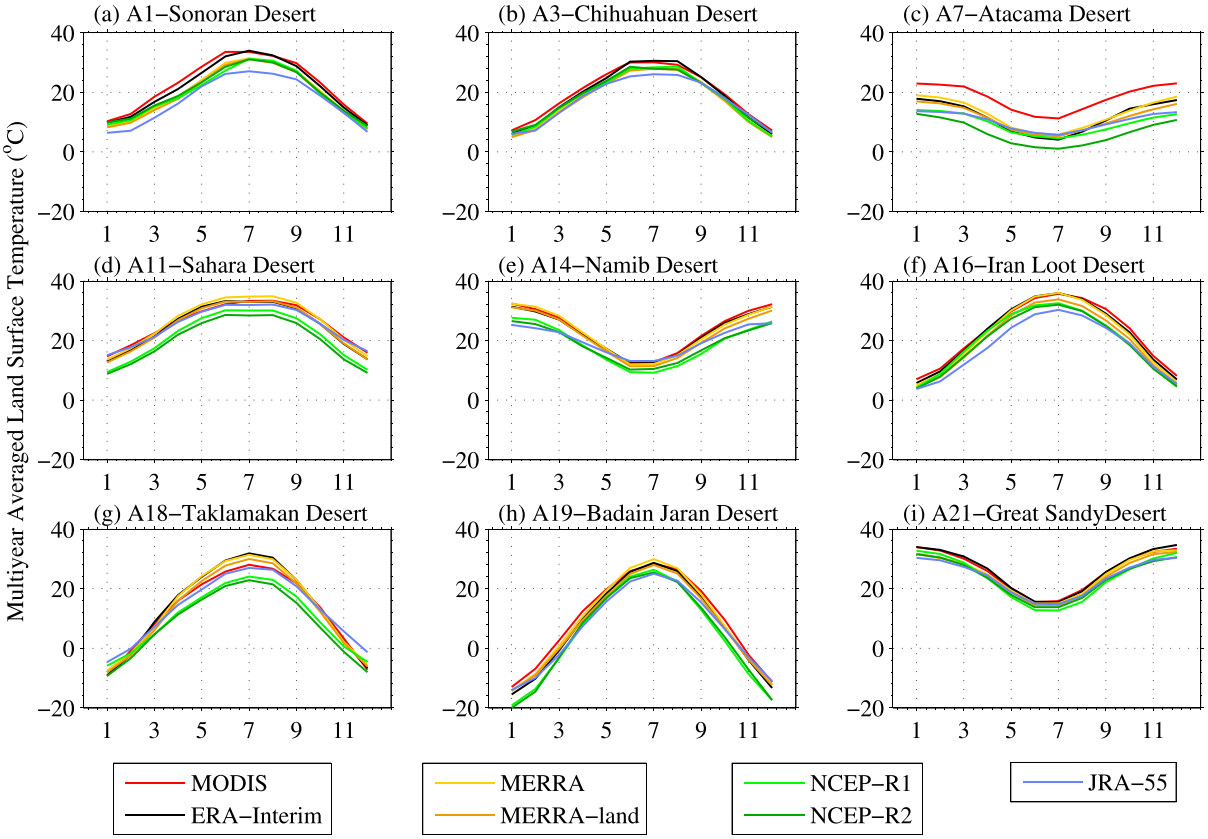

Figure 3. Multiyear averaged monthly mean land surface temperatures (LSTs) of the corrected MODIS data and reanalysis data, including ERA-Interim, MERRA, MERRA land, NCEP-R1, NCEP-R2, and JRA-55, for nine subregions. LSTs from August 2002 to August 2015 were used, except for JRA-55, which are only from August 2002 to December 2013. These nine region samples are uniformly distributed over arid/desert and semiarid regions, i.e., the American Midwest, northern Chile, the Sahara Desert, southern Africa, midwestern Asia, the Taklimakan Desert, and Australia (see Figure 1). The reanalysis LST data have seasonal cycles nearly identical to those of the MODIS data.

To use T_{MODIS} to compare the LST output of the reanalyses, we directly correlated T_{MODIS} with T_{all} calculated from the USCRN sites (Figure 2c). In all, the error in T_{MODIS} relative to T_{all} totals 1.36°C (±1.83°C STD), mainly resulting from the impact of cloud status and sample error in the four daily measurements (Figure 2c). This error must be corrected. Fortunately, T_{all} is linearly related to T_{MODIS}, which makes it easy to correct T_{MODIS} with the linear regression equation of T_{all} against T_{MODIS} (Figure 2c) to evaluate the reanalysis output of the monthly mean LST data.

MODIS LST is only available under clear conditions, whereas the reanalysis LSTs are available under all conditions including clear- and cloudy-sky conditions. In this study, we used the bias-corrected MODIS LST to compare the LSTs simulated by current reanalyses because (1) the availability of MODIS LST is more than 94% over deserts (Figure 1), (2) we corrected the impact of cloud on mean values of MODIS LST, and (3) cloud frequency from MODIS over desert has no significant trend during the study period ($p = 0.5$, Figure S1), which might not introduce significant biases into the trends between MODIS and reanalysis LSTs.

3.2. Mean State of Land Surface Temperatures Over Arid Regions

Based on the corrected MODIS LST, we examined mean state of LSTs in reanalyses involving ERA-Interim, JRA-55, MERRA, MERRA-land, NCEP-R1, and NCEP-R2 from August 2002 to August 2015 in nine subregions (shown in Figure 1) over global deserts. We found that the reanalyses capture the seasonal cycles in LST (Figure 3). This seasonality is evident over desert regions, with the maximum LST in July and the minimum LST in January (Figure 3). However, the multiyear averaged LSTs largely differ among the reanalyses. Relative to the corrected MODIS LST, ERA-Interim, MERRA, and MERRA-land overestimate LST by an average of 0.66°C (0.85°C STD), whereas JRA-55, NCEP-R1, and NCEP-R2 underestimate LST by an average of −1.68°C

Table 2. The Multiyear Averages and Annual Temperature Ranges (ATR) of Land Surface Temperature (LST) and the Biases and Standard Deviations (STD) Compared With Corrected MODIS LST Data[a]

	Semiarid Regions						Arid/Desert Regions					
	Mean	ATR	Bias	STD	*R***	Trend	Mean	ATR	Bias	STD	*R***	Trend
MODIS	19.19	8.84	-	-	-	0.07	23.45	12.74	-	-	-	0.25**
ERA-Interim	19.32	9.19	0.13	0.38	0.93	0.01	24.47	14.39	1.02	0.84	0.87	−0.07
MERRA	19.42	9.24	0.23	0.37	0.89	0.04	24.40	14.96	0.95	1.02	0.87	0.10
MERRA-land	19.02	8.84	−0.17	0.37	0.90	−0.04	23.47	14.53	0.02	0.90	0.88	0.10
JRA-55	18.93	8.12	−0.22	0.34	0.89	−0.31*	23.00	12.52	−0.42	0.55	0.89	−0.14
NCEP-R1	17.32	8.64	−1.87	0.48	0.86	−0.05	21.49	13.95	−1.96	0.92	0.82	0.05
NCEP-R2	17.66	8.62	−1.52	0.42	0.89	−0.12	20.80	13.84	−2.65	0.86	0.84	−0.06

[a]The correlation coefficients (*R*) and trends of the LST anomalies are relative to the entire period from August 2002 to August 2015 over arid/desert and semiarid regions. Note that the time span of JRA-55 ends in December 2013. LSTs from the corrected MODIS and reanalyses, including ERA-Interim, JRA-55, MERRA, MERRA-land, NCEP-R1, and NCEP-R2, were used. Note that the time span of JRA-55 ends in December 2013.
*0.05.
**0.01.

(0.78°C STD) in arid/desert regions (Table 2). These differences decrease to 0.06°C (0.37°C STD) in the former group and −1.20°C (0.41°C STD) in the latter group over semiarid regions (Table 2). These biases were suggested to correlate with a misrepresentation of surface energy fluxes in those areas [*Trigo et al.,* 2015].

Reanalyses use default broadband emissivity based on land cover types to calculate LST. However, emissivity exhibits considerable spatial variability over deserts and depends on the physical and chemical characteristics of desert surfaces [*Li et al.,* 2011, 2013b; *Tsvetsinskaya et al.,* 2002; *Wang et al.,* 2005; *Zhou et al.,* 2003].

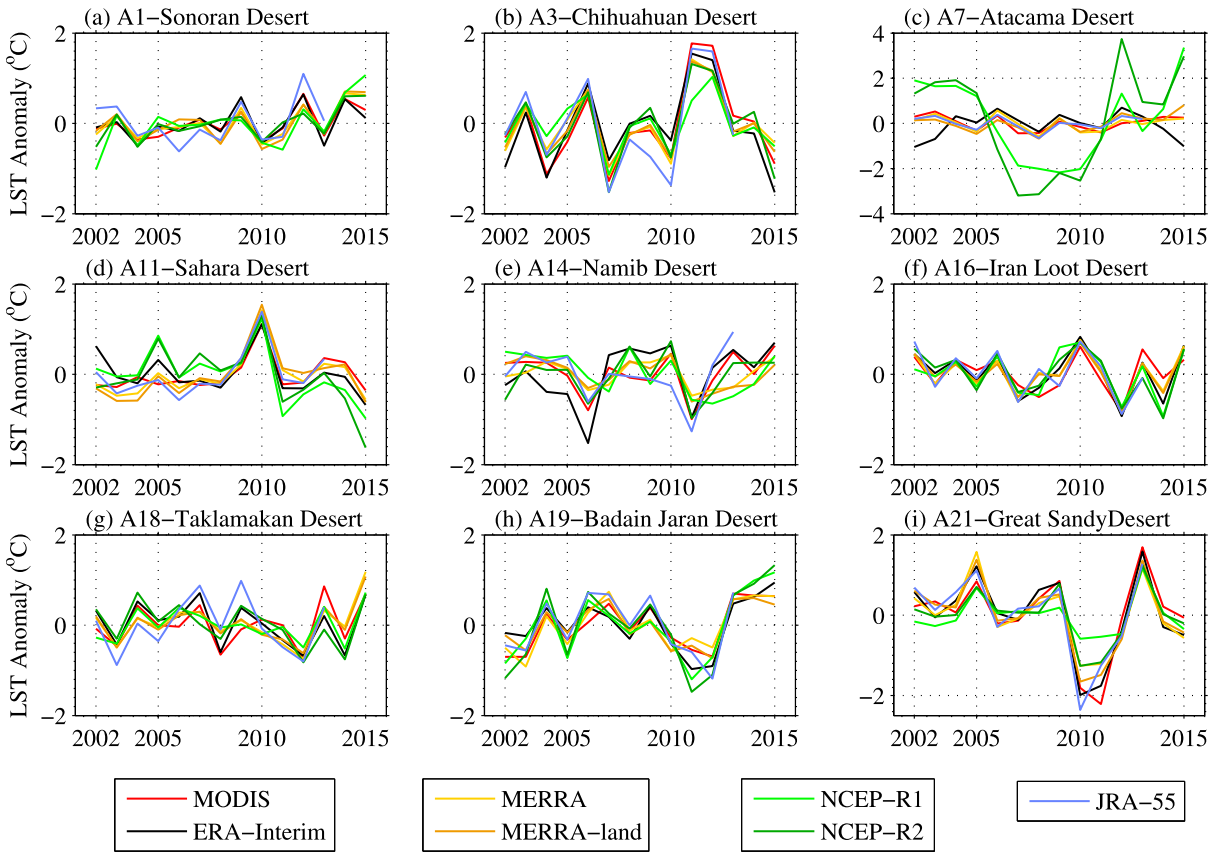

Figure 4. (a–i) The annual LST anomalies relative to the entire period, from MODIS and the reanalyses. The reanalysis data include ERA-Interim, MERRA, MERRA land, NCEP-R1, NCEP-R2, and JRA-55.

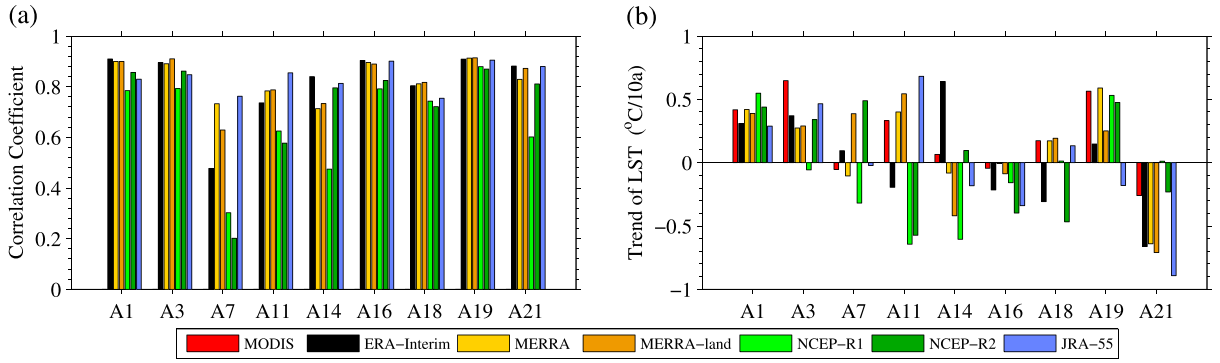

Figure 5. (a) The correlation coefficients (*R*) of the reanalysis LST monthly anomalies versus the MODIS LST anomaly. (b) The linear trends (unit: °C/10 a) in the LST anomalies from MODIS and reanalysis data. The reanalysis data include ERA-Interim, MERRA, MERRA land, NCEP-R1, NCEP-R2, and JRA-55.

This variability may introduce biases into the LST data from the reanalyses. In addition, the bias of reanalysis LST may be also related to how the reanalyses handle the surface analysis from the model output of the lowest level of the atmosphere. Besides, model representation of the surface-atmosphere couplings and model input of forcing data (including radiative forcing and precipitation) are responsible. The annual LST range (ATR) in the reanalyses is larger by 1.60°C than that in MODIS for arid/desert regions, with the exception of the ATR of JRA-55, which is smaller by 0.22°C (Table 2). Note that the LST estimation accuracy of MERRA-land is better than that of MERRA (the bias is lower by 0.93°C and the STD by 0.1°C; Table 2) due to the inclusion of precipitation forcing data.

3.3. Annual Variability and Trends of Land Surface Temperature Over Deserts

Figure 4 shows the annual LST anomalies relative to the entire period of 2002–2015. The interannual variability in LST anomalies in the reanalyses is synchronized, but the magnitudes of the LST anomalies are notably

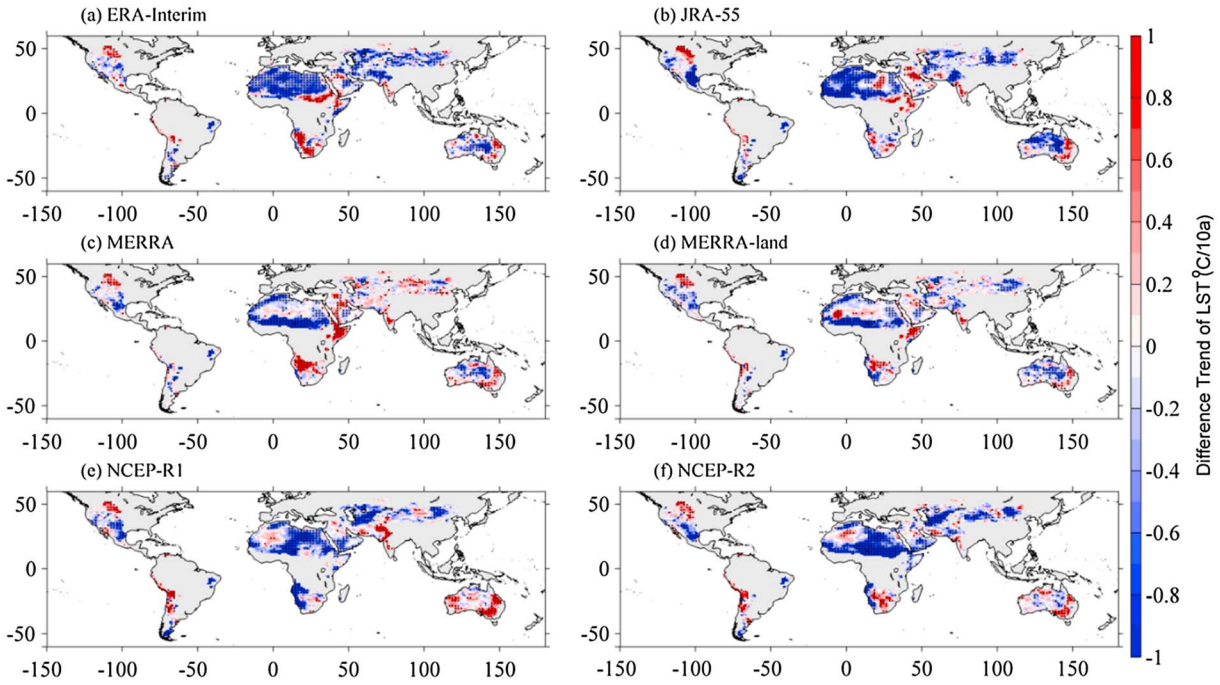

Figure 6. Spatial map of the trends in the LST differences, i.e., reanalyses minus MODIS, at 1° × 1° latitude/longitude grids over arid/desert and semiarid regions (unit: °C/10 a). The dots denote trends with statistical significance at a significance level of 0.1. The reanalysis data include (a) ERA-Interim, (b) JRA-55, (c) MERRA, (d) MERRA-land, (e) NCEP-R1, and (f) NCEP-R 2. Note that the time span of JRA-55 ends in December 2013. The trends of their differences were calculated with linear regression and Student's *t* test.

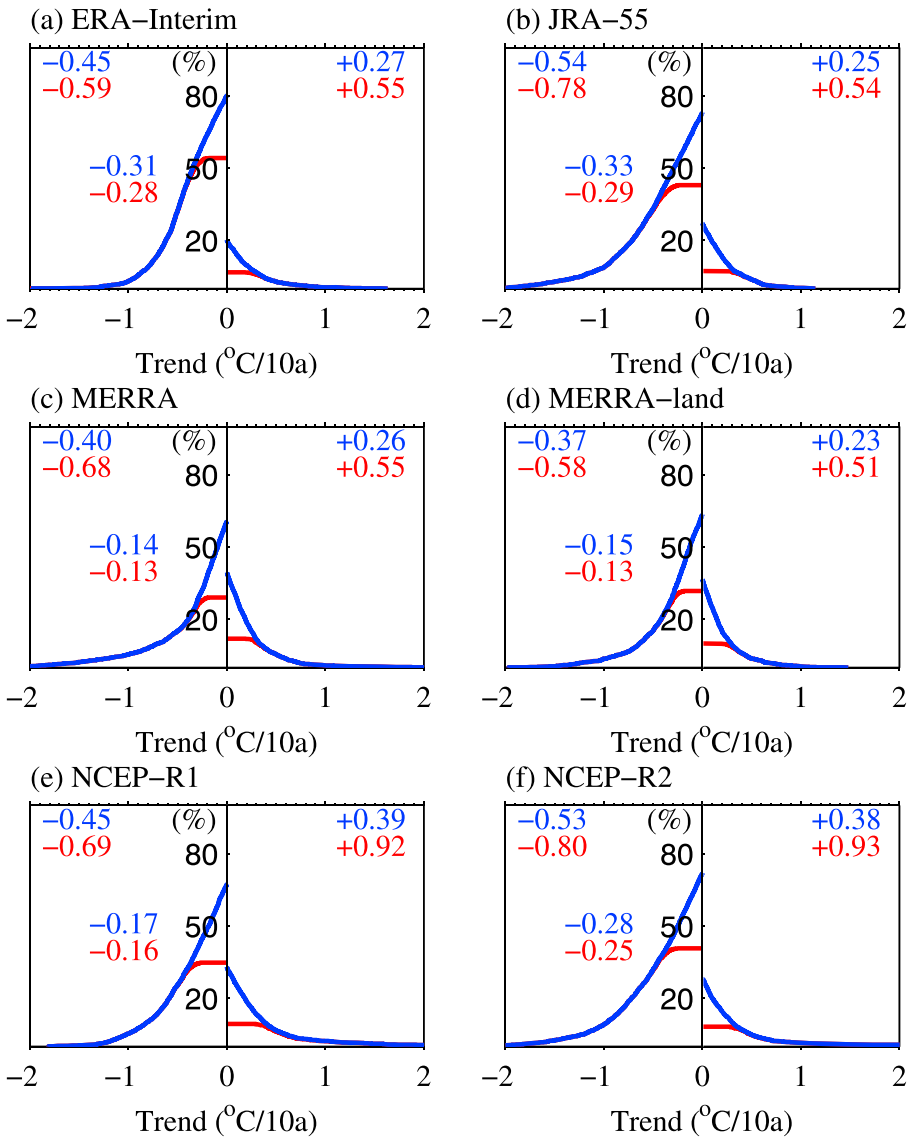

Figure 7. Cumulative frequency distributions of the LST trend difference (reanalysis minus MODIS) at 1° × 1°grids of deserts (unit: °C/10 a). The reanalysis data include (a) ERA-Interim, (b) JRA-55, (c) MERRA assimilation, (d) MERRA-land simulation, (e) NCEP-R1, and (f) NCEP-R2. For positive trends (right column in each subfigure), the frequency is cumulative to +2°C/10 a, whereas for negative trends (left column in each subfigure), the frequency is cumulative to −2°C/10 a. The blue line is the cumulative frequency of all the trends (averaged value in blue), whereas the red line is for the trends with a statistical significance level of 0.1 (averaged value in red). The trends of their differences were calculated with linear regression and Student's *t* test.

different and more or less exceed the MODIS LST anomaly (Figure 4), mainly due to the imprecisely simulated effects of the natural climate variability of the Earth on LSTs in state-of-the-art reanalyses. In addition, NCEP-R1 and NCEP-R2 cannot capture the LST anomaly in A7 of the Atacama (Figure 4a), owning Earth's surface solar radiation maximum [*Rondanelli et al.,* 2014]. This failure may be related to an inaccurate surface incident radiation in the models [*Ma et al.,* 2015] induced by the complex terrain (ranging from 240 m to 6346 m with an average of approximately 2600 m across A7) and atmospheric conditions [*Rondanelli et al.,* 2014].

Although reanalysis LST anomalies correlate well with the MODIS LST anomalies (with an average *R* of approximately 0.82 in eight sample regions), the MODIS and reanalysis trends exhibit many inconsistencies, including very large differences or opposite signs (Figure 5). Specifically, MODIS LST does own significant

linear trends especially in most deserts, but Reanalyses LST do not (Figure S2). The similar result was obtained based on Theil-Sen's trend estimator [*Sen*, 1968; *Theil*, 1992] and Mann-Kendal trend test [*Kendall*, 1948; *Mann*, 1945] (Figure S3, detailed method in online supporting information). The correlation coefficients of the LST anomalies between MODIS and reanalyses are 0.82–0.89 over global arid/desert regions and 0.86–0.93 over global semiarid regions (Table 2). Nevertheless, the increasing trend in MODIS LST (0.25°C/decade, $p < 0.01$) over arid/desert regions remains far higher than those from all of the reanalyses, which vary from −0.14 to 0.1°C/decade from 2002 to 2015 (Table 2).

Our results provide independent evidence for an amplified warming from LST over deserts, which is consistent with the findings of previous studies demonstrating a warming amplification from LSAT since 1979 over deserts [*Zhou et al.,* 2015]. Table 2 shows that deserts have a mean warming rate of 0.25°C/decade ($p < 0.01$) compared with a warming rate of 0.07°C/decade over adjacent semiarid regions (Table 2). This finding reminds us to be cautious when extrapolating global warming based on LSAT data sets to areas with limited data, such as deserts. Dynamic effects induced by Earth's internal variabilities [*Wallace et al.,* 2012] and radiative effects from anthropogenic greenhouse gases and dust aerosols [*Guan et al.,* 2016], etc. have been put forward to explain the warming amplification in the drylands [*Guan et al.,* 2015a, 2015b]. The CO_2 radiative forcing and its effect on circulation change were suggested to be stronger under dry atmosphere and infrequent clouds [*Merlis*, 2015].

To better interpret the trend discrepancy in the reanalyses, Figure 6 shows a spatial map of the trends in the LST anomaly differences between MODIS and the reanalyses. Underestimated trends with statistical significance at a level of 0.1 are centered in North American deserts, the Sahara Desert, the Taklimakan Desert, midwestern Asia, and Australia (Figure 6). The similar result was obtained based on Theil-Sen's trend estimator [*Sen*, 1968; *Theil*, 1992] and Mann-Kendal trend test [*Kendall*, 1948; *Mann*, 1945] (Figure S4). Figure 7 shows the cumulative frequency distributions of the departure trends in the reanalysis LST anomalies at $1° \times 1°$ latitude/longitude grids over arid/desert regions. The figure reveals that the LST trend underestimation in the reanalyses occurs in up to 70% of global deserts (−0.46°C/decade averaged from all reanalyses, as are the values below), with statistical significance in approximately 40% of deserts (−0.69°C/decade); in the remaining 30% of global deserts, the LST trend is overestimated (0.30°C/decade), with statistical significance in nearly 9% of deserts (0.67°C/decade) (Figure 7). Therefore, the trends of the reanalyses are aggregated to be underestimated by −0.14 to −0.32°C/decade over global deserts (−0.23°C/decade) (Figure 7). The similar result was obtained based on Theil-Sen's trend estimator [*Sen*, 1968; *Theil*, 1992] and Mann-Kendal trend test [*Kendall*, 1948; *Mann*, 1945] (Figure S5).

4. Conclusions and Discussion

Instead of station-based LSAT that is globally distributed but scarce in deserts [*Zhou and Wang,* 2016b, 2016d], satellite-derived LST data feature truly global coverage and make it possible to examine the accuracy of reanalysis LSTs, especially in arid/desert and semiarid regions with a high degree of cloudlessness.

Compared to T_{all}, averaged from all the 5 min measurements, MODIS LSTs have a total error of 1.36°C (±1.83°C STD) due to the impact of cloud status and sample error in the four daily measurements. This error in T_{MODIS} can be corrected using the linear relationship with T_{all}, which helps to evaluate the reanalysis output of monthly mean LST.

After removal of the bias of MODIS LST, the mean state, variability, and trends in the reanalysis LST products have been validated. The seasonal cycle and interannual variability of LST can be reproduced by the reanalyses, but the multiyear LST mean has considerable uncertainty, i.e., overestimation (average: 0.66°C) by the ERA-Interim, MERRA, and MERRA-land models and underestimation (average: −1.68°C) by the JRA-55, NCEP-R1, and NCEP-R2 models over arid/desert regions. Furthermore, the MODIS LST trend averaged over global deserts (0.25°C/decade) is far larger than those of the reanalyses (−0.14 to 0.10°C/decade) for the 2002–2015 period. The underestimation of the LST trend by the reanalyses can be detected in approximately 70% of the global deserts. Our results provide independent evidence for an amplified warming (0.25°C/decade, $p < 0.01$) from LST over global deserts and a warming rate of just 0.07°C/decade over adjacent semiarid regions, which is consistent with the findings of previous studies that showed a warming amplification from LSAT since 1979 over deserts [*Zhou et al.,* 2015].

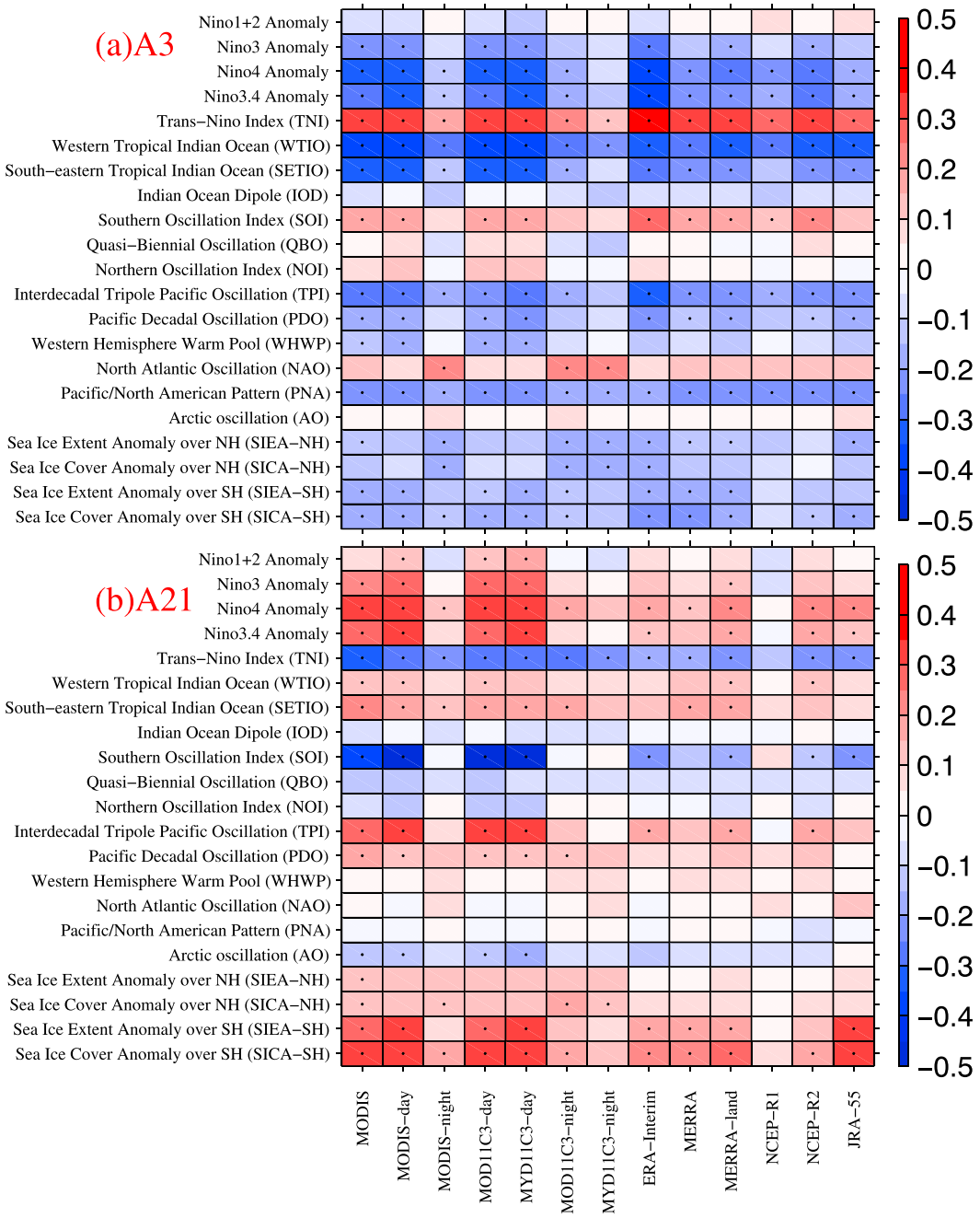

Figure 8. Correlation coefficients of MODIS and reanalysis LST monthly anomalies (after linearly detrending) versus surface ocean indices (including the Pacific, Indian, and Atlantic Oceans), atmospheric teleconnection, and sea ice indices over the regions A3 (in the (a) Northern Hemisphere) and A21 (in the (b) Southern Hemisphere). A black dot within the grid box signifies the passing of a *t* test at a significance level of 0.1. The data from MODIS include the corrected monthly MODIS LST, daytime MODIS LST, nighttime MODIS LST and four daily MODIS LSTs per month. The reanalysis data include ERA-Interim, MERRA, MERRA-land, NCEP-R1, NCEP-R2, and JRA-55.

Reanalyses can provide the best possible analysis of both observed (e.g., surface air temperature and relative humidity) and unobserved parameters (e.g., potential vorticity and soil moisture) and can provide complete spatiotemporal and physical features at each time point [*Dee et al.,* 2011b; *Zhou and Wang*, 2016c]. However, whether reanalyses can reconstruct the long-term homogeneous trends remains uncertain [*Dee et al.,* 2011a; *Thorne and Vose*, 2010]. Our study provides a way to evaluate the trend estimated by reanalyses based on

satellite-derived data and reveals that substantial improvement is needed for the existing reanalysis models to produce LSTs for climate change studies.

Several studies were conducted to link change in LST with atmospheric circulations. For examples, *Lensky and Dayan* [2015] attempted to quantify the impact of several atmospheric circulations on LST patterns over East Mediterranean using 2000–2012 MODIS data. *Zhuo et al.* [2016] investigated the interactions between LST and atmospheric circulations over China by Weather Research and Forecasting model. Therefore, change in LST, especially in deserts, may be modulated by several Earth system variables including surface ocean circulations, atmosphere teleconnections, and sea ice change, and be coupled with land-atmosphere interactions including the partitioning of surface available energy and surface longwave radiation under different surface and atmospheric conditions [*Wang and Dickinson,* 2012, 2013].

Here we preliminarily pointed out the discrepancy in responses of Reanalysis and MODIS LSTs to various Earth system variables by selecting two representative regions, i.e., A3 and A21. The ERA-Interim model can roughly capture the effect of natural variability on the LST anomaly in the A3 region but not in the A21 region (Figure 8). However, the other reanalyses have considerable difficulty in effectively simulating the relationships between LST anomalies and Earth's internal variability (Figure 8). This universally underestimated dependence in the reanalyses (relative to MODIS data) reveals the need for considerable improvement in this aspect.

We further found that daytime and nighttime LSTs are affected by different variables and that the effect of these variables on daytime LSTs is much stronger than that on nighttime LSTs throughout the sample regions (Figures 8 and S6). Therefore, the mechanisms by which the responsible processes influence the daytime and nighttime LSTs are obviously different, and this asymmetric effect should be considered and included in reanalysis models to achieve higher-accuracy outputs.

Acknowledgments

This study was funded by the National Natural Science Foundation of China (41525018 and 91337111) and the National (2012CB955302). Considerable gratitude is owed to the moderate resolution imaging spectroradiometer (MODIS) land team (http://modis.gsfc.nasa.gov), several reanalysis working teams including the European Centre for Medium-Range Weather Forecasts (ECMWF) for providing ERA-Interim data (http://www.ecmwf.int/), the Global Modeling and Assimilation Office (GMAO) at NASA Goddard Space Flight Center for MERRA data (http://gmao.gsfc.nasa.gov/merra/), Physical Sciences Division (PSD) of NOAA Earth System Research Laboratory (ESRL) for NCEP data (http://www.esrl.noaa.gov/psd/), and Climate Prediction Division of Global Environment and Marine Department in Japan Meteorological Agency for JRA-55 data (http://jra.kishou.go.jp/). We feel very grateful to National Snow and Ice Data Center (NSIDC, http://nsidc.org/) for providing available sea ice index and to Earth System Research Laboratory of NOAA (http://www.esrl.noaa.gov/) for surface ocean indices, atmospheric teleconnection indices, and the ground-based LST from the U.S. Climate Reference Network (USCRN).

References

Baldwin, M. P., et al. (2001), The quasi-biennial oscillation, *Rev. Geophys.*, *39*, 179–229, doi:10.1029/1999RG000073.

Barnston, A. G., and R. E. Livezey (1987), Classification, seasonality and persistence of low-frequency atmospheric circulation patterns, *Mon. Weather Rev.*, *115*(6), 1083–1126, doi:10.1175/1520-0493(1987)115<1083:CSAPOL>2.0.CO;2.

Best, M., A. Beljaars, J. Polcher, and P. Viterbo (2004), A proposed structure for coupling tiled surfaces with the planetary boundary layer, *J. Hydrometeorol.*, *5*(6), 1271–1278.

Blunden, J., and D. S. Arndt (2015), State of the climate in 2014, *Bull. Am. Meteorol. Soc.*, *96*(7), ES1–ES32, doi:10.1175/2015BAMSStateoftheClimate.1.

Briegleb, B., and V. Ramanathan (1982), Spectral and diurnal variations in clear sky planetary albedo, *J. Appl. Meteorol.*, *21*(8), 1160–1171.

Chang, P., L. Ji, and H. Li (1997), A decadal climate variation in the tropical Atlantic Ocean from thermodynamic air-sea interactions, *Nature*, *385*(6616), 516–518.

Chiang, J. C. H., and D. J. Vimont (2004), Analogous Pacific and Atlantic meridional modes of tropical atmosphere–ocean variability, *J. Clim.*, *17*(21), 4143–4158, doi:10.1175/JCLI4953.1.

Chou, M.-D., and K.-T. Lee (1996), Parameterizations for the absorption of solar radiation by water vapor and ozone, *J. Atmos. Sci.*, *53*(8), 1203–1208.

Coll, C., V. Caselles, J. M. Galve, E. Valor, R. Niclos, J. M. Sanchez, and R. Rivas (2005), Ground measurements for the validation of land surface temperatures derived from AATSR and MODIS data, *Remote Sens. Environ.*, *97*(3), 288–300, doi:10.1016/j.rse.2005.05.007.

Coll, C., Z. M. Wan, and J. M. Galve (2009), Temperature-based and radiance-based validations of the V5 MODIS land surface temperature product, *J. Geophys. Res.*, *114*, D20102, doi:10.1029/2009JD012038.

Cowtan, K., and R. G. Way (2014), Coverage bias in the HadCRUT4 temperature series and its impact on recent temperature trends, *Q. J. R. Meteorol. Soc.*, *140*(683), 1935–1944, doi:10.1002/qj.2297.

Dee, D. P., E. Källén, A. J. Simmons, and L. Haimberger (2011a), Comments on "Reanalyses suitable for characterizing long-term trends", *Bull. Am. Meteorol. Soc.*, *92*(1), 65–70, doi:10.1175/2010BAMS3070.1.

Dee, D. P., et al. (2011b), The ERA-Interim reanalysis: Configuration and performance of the data assimilation system, *Q. J. R. Meteorol. Soc.*, *137*(656), 553–597, doi:10.1002/qj.828.

Dee, D. P., M. Balmaseda, G. Balsamo, R. Engelen, A. J. Simmons, and J. N. Thépaut (2014), Toward a consistent reanalysis of the climate system, *Bull. Am. Meteorol. Soc.*, *95*(8), 1235–1248, doi:10.1175/bams-d-13-00043.1.

Diamond, H. J., T. R. Karl, M. A. Palecki, C. B. Baker, J. E. Bell, R. D. Leeper, D. R. Easterling, J. H. Lawrimore, T. P. Meyers, and M. R. Helfert (2013), US Climate Reference Network after one decade of operations: Status and assessment, *Bull. Am. Meteorol. Soc.*, *94*(4), 485–498.

Enfield, D. B., A. M. Mestas-Nuñez, D. A. Mayer, and L. Cid-Serrano (1999), How ubiquitous is the dipole relationship in tropical Atlantic sea surface temperatures?, *J. Geophys. Res.*, *104*, 7841–7848, doi:10.1029/1998JC900109.

Ezcurra, E. (2006), *Global Deserts Outlook 2006, Global Environment Outlook (GEO) Series of the United Nations Environment Programme (UNEP)*, Earthprint Nairobi, Kenya. [Available at http://www.earthprint.com.]

Gallo, K., R. Hale, D. Tarpley, and Y. Yu (2011), Evaluation of the relationship between air and land surface temperature under clear- and cloudy-sky conditions, *J. Appl. Meteorol. Climatol.*, *50*(3), 767–775, doi:10.1175/2010JAMC2460.1.

Guan, X., J. Huang, R. Guo, and P. Lin (2015a), The role of dynamically induced variability in the recent warming trend slowdown over the Northern Hemisphere, *Sci. Rep.*, *5*, 12,669, doi:10.1038/srep12669.

Guan, X., J. Huang, R. Guo, H. Yu, P. Lin, and Y. Zhang (2015b), Role of radiatively forced temperature changes in enhanced semi-arid warming in the cold season over east Asia, *Atmos. Chem. Phys.*, *15*(23), 13,777–13,786, doi:10.5194/acp-15-13777-2015.

Guan, X., J. Huang, Y. Zhang, Y. Xie, and J. Liu (2016), The relationship between anthropogenic dust and population over global semi-arid regions, *Atmos. Chem. Phys.*, *16*(8), 5159–5169, doi:10.5194/acp-16-5159-2016.

Halpert, M. S., and G. D. Bell (1997), Climate assessment for 1996, *Bull. Am. Meteorol. Soc.*, *78*(5), 1038, doi:10.1175/1520-0477(1997)078<1038:CAF>2.0.CO;2.

Hansen, J., R. Ruedy, J. Glascoe, and M. Sato (1999), GISS analysis of surface temperature change, *J. Geophys. Res.*, *104*, 30,997–31,022, doi:10.1029/1999JD900835.

Harris, I., P. D. Jones, T. J. Osborn, and D. H. Lister (2014), Updated high-resolution grids of monthly climatic observations—The CRU TS3.10 dataset, *Int. J. Climatol.*, *34*(3), 623–642, doi:10.1002/joc.3711.

Henley, B., J. Gergis, D. Karoly, S. Power, J. Kennedy, and C. Folland (2015), A tripole index for the Interdecadal Pacific Oscillation, *Clim. Dyn.*, *45*(11), 3077–3090, doi:10.1007/s00382-015-2525-1.

Hong, S.-Y., and H.-L. Pan (1996), Nonlocal boundary layer vertical diffusion in a medium-range forecast model, *Mon. Weather Rev.*, *124*(10), 2322–2339.

Huang, J., X. Guan, and F. Ji (2012), Enhanced cold-season warming in semi-arid regions, *Atmos. Chem. Phys.*, *12*(12), 5391–5398, doi:10.5194/acp-12-5391-2012.

Huang, J., H. Yu, X. Guan, G. Wang, and R. Guo (2015), Accelerated dryland expansion under climate change, *Nat. Clim. Change*, *6*(2), 166–171, doi:10.1038/nclimate2837.

Hubbard, K. G., X. Lin, and C. B. Baker (2005), On the USCRN temperature system, *J. Atmos. Oceanic Technol.*, *22*(7), 1095–1101, doi:10.1175/Jtech1715.1.

Intergovernmental Panel on Climate Change (IPCC) (2013), *Climate Change 2013: The Physical Science Basis. Contribution of Working Group I to the Fifth Assessment Report of the Intergovernmental Panel on Climate Change*, edited by T. F. Stocker et al., Cambridge Univ. Press, New York.

Kalnay, E., M. Kanamitsu, R. Kistler, W. Collins, D. Deaven, L. Gandin, M. Iredell, S. Saha, G. White, and J. Woollen (1996), The NCEP/NCAR 40-year reanalysis project, *Bull. Am. Meteorol. Soc.*, *77*(3), 437–471.

Kanamitsu, M., W. Ebisuzaki, J. Woollen, S.-K. Yang, J. J. Hnilo, M. Fiorino, and G. L. Potter (2002), NCEP–DOE AMIP-II Reanalysis (R-2), *Bull. Am. Meteorol. Soc.*, *83*(11), 1631–1643, doi:10.1175/BAMS-83-11-1631.

Karl, T. R., A. Arguez, B. Huang, J. H. Lawrimore, J. R. McMahon, M. J. Menne, T. C. Peterson, R. S. Vose, and H.-M. Zhang (2015), Possible artifacts of data biases in the recent global surface warming hiatus, *Science*, *348*(6242), 1469–1472, doi:10.1126/science.aaa5632.

Kendall, M. G. (1948), *Rank Correlation Methods*, Griffin, Oxford, U. K.

Kobayashi, S., et al. (2015), The JRA-55 reanalysis: General specifications and basic characteristics, *J. Meteorol. Soc. Jpn.*, *93*(1), 5–48, doi:10.2151/jmsj.2015-001.

Kottek, M., J. Grieser, C. Beck, B. Rudolf, and F. Rubel (2006), World map of the Koppen-Geiger climate classification updated, *Meteorol. Z.*, *15*(3), 259–263.

Lawrimore, J. H., M. J. Menne, B. E. Gleason, C. N. Williams, D. B. Wuertz, R. S. Vose, and J. Rennie (2011), An overview of the Global Historical Climatology Network monthly mean temperature data set, version 3, *J. Geophys. Res.*, *116*, D19121, doi:10.1029/2011JD016187.

Lensky, I. M., and U. Dayan (2015), Satellite observations of land surface temperature patterns induced by synoptic circulation, *Int. J. Climatol.*, *35*(2), 189–195.

Li, J., Z. L. Li, X. Jin, T. J. Schmit, L. H. Zhou, and M. D. Goldberg (2011), Land surface emissivity from high temporal resolution geostationary infrared imager radiances: Methodology and simulation studies, *J. Geophys. Res.*, *116*, D01304, doi:10.1029/2010JD014637.

Li, Z.-L., B.-H. Tang, H. Wu, H. Ren, G. Yan, Z. Wan, I. F. Trigo, and J. A. Sobrino (2013a), Satellite-derived land surface temperature: Current status and perspectives, *Remote Sens. Environ.*, *131*, 14–37, doi:10.1016/j.rse.2012.12.008.

Li, Z.-L., H. Wu, N. Wang, S. Qiu, J. A. Sobrino, Z. M. Wan, B. H. Tang, and G. J. Yan (2013b), Land surface emissivity retrieval from satellite data, *Int. J. Remote Sens.*, *34*(9–10), 3084–3127, doi:10.1080/01431161.2012.716540.

Lim, Y. K., M. Cai, E. Kalnay, and L. M. Zhou (2005), Observational evidence of sensitivity of surface climate changes to land types and urbanization, *Geophys. Res. Lett.*, *32*, L22712, doi:10.1029/2005GL024267.

Ma, Q., K. C. Wang, and M. Wild (2015), Impact of geolocations of validation data on the evaluation of surface incident shortwave radiation from Earth System Models, *J. Geophys. Res. Atmos.*, *120*, 6825–6844, doi:10.1002/2014JD022572.

Mann, H. B. (1945), Nonparametric tests against trend, *Econometrica*, *13*(3), 245–259.

Merlis, T. M. (2015), Direct weakening of tropical circulations from masked CO_2 radiative forcing, *Proc. Natl. Acad. Sci. U.S.A.*, *112*(43), 13,167–13,171, doi:10.1073/pnas.1508268112.

Reichle, R. H., R. D. Koster, G. J. M. De Lannoy, B. A. Forman, Q. Liu, S. P. P. Mahanama, and A. Touré (2011), Assessment and enhancement of MERRA land surface hydrology estimates, *J. Clim.*, *24*(24), 6322–6338, doi:10.1175/JCLI-D-10-05033.1.

Rienecker, M. M., et al. (2011), MERRA: NASA's Modern-Era Retrospective Analysis for Research and Applications, *J. Clim.*, *24*(14), 3624–3648, doi:10.1175/JCLI-D-11-00015.1.

Rondanelli, R., A. Molina, and M. Falvey (2014), The Atacama surface solar maximum, *Bull. Am. Meteorol. Soc.*, *96*(3), 405–418, doi:10.1175/BAMS-D-13-00175.1.

Rotenberg, E., and D. Yakir (2010), Contribution of semi-arid forests to the climate system, *Science*, *327*(5964), 451–454.

Salomonson, V. V., W. Barnes, P. W. Maymon, H. E. Montgomery, and H. Ostrow (1989), MODIS: Advanced facility instrument for studies of the Earth as a system, *IEEE Trans. Geosci. Remote Sens.*, *27*(2), 145–153.

Schwing, F. B., T. Murphree, and P. M. Green (2002), The Northern Oscillation Index (NOI): A new climate index for the northeast Pacific, *Prog. Oceanogr.*, *53*(2–4), 115–139, doi:10.1016/S0079-6611(02)00027-7.

Sen, P. K. (1968), Estimates of the regression coefficient based on Kendall's tau, *J. Am. Stat. Assoc.*, *63*(324), 1379–1389, doi:10.2307/2285891.

Sobrino, J. A., and Y. Julien (2013), Trend analysis of global MODIS-Terra vegetation indices and land surface temperature between 2000 and 2011, *IEEE J. Sel. Top. Appl. Earth Obs. Remote Sens.*, *6*(5), 2139–2145.

Theil, H. (1992), A rank-invariant method of linear and polynomial regression analysis, in *Henri Theil's Contributions to Economics and Econometrics: Econometric Theory and Methodology*, edited by B. Raj and J. Koerts, pp. 345–381, Springer, Dordrecht, Netherlands.

Thorne, P., and R. Vose (2010), Reanalyses suitable for characterizing long-term trends: Are they really achievable?, *Bull. Am. Meteorol. Soc.*, *91*(3), 353–361.

Tomlinson, C. J., L. Chapman, J. E. Thornes, and C. Baker (2011), Remote sensing land surface temperature for meteorology and climatology: A review, *Meteorol. Appl.*, *18*(3), 296–306, doi:10.1002/met.287.

Trenberth, K. E. (1984), Signal versus noise in the Southern Oscillation, *Mon. Weather Rev.*, *112*(2), 326–332, doi:10.1175/1520-0493(1984)112<0326:SVNITS>2.0.CO;2.

Trenberth, K. E., and J. Hurrell (1994), Decadal atmosphere-ocean variations in the Pacific, *Clim. Dyn.*, *9*(6), 303–319, doi:10.1007/BF00204745.

Trenberth, K. E., and D. P. Stepaniak (2001), Indices of El Niño evolution, *J. Clim.*, *14*(8), 1697–1701, doi:10.1175/1520-0442(2001)014<1697:LIOENO>2.0.CO;2.

Trigo, I., S. Boussetta, P. Viterbo, G. Balsamo, A. Beljaars, and I. Sandu (2015), Comparison of model land skin temperature with remotely sensed estimates and assessment of surface-atmosphere coupling, *J. Geophys. Res. Atmos.*, *120*, 12,096–12,111, doi:10.1002/2015JD023812.

Tsvetsinskaya, E. A., C. B. Schaaf, F. Gao, A. H. Strahler, R. E. Dickinson, X. Zeng, and W. Lucht (2002), Relating MODIS-derived surface albedo to soils and rock types over Northern Africa and the Arabian peninsula, *Geophys. Res. Lett.*, *29*(9), 1353, doi:10.1029/2001GL014096.

Wallace, J. M., and D. S. Gutzler (1981), Teleconnections in the geopotential height field during the Northern Hemisphere Winter, *Mon. Weather Rev.*, *109*(4), 784–812, doi:10.1175/1520-0493(1981)109<0784:TITGHF>2.0.CO;2.

Wallace, J. M., Q. Fu, B. V. Smoliak, P. Lin, and C. M. Johanson (2012), Simulated versus observed patterns of warming over the extratropical Northern Hemisphere continents during the cold season, *Proc. Natl. Acad. Sci. U.S.A.*, *109*(36), 14,337–14,342, doi:10.1073/pnas.1204875109.

Wan, Z. M., and Z.-L. Li (1997), A physics-based algorithm for retrieving land-surface emissivity and temperature from EOS/MODIS data, *IEEE Trans. Geosci. Remote Sens.*, *35*(4), 980–996, doi:10.1109/36.602541.

Wan, Z. M., and Z.-L. Li (2008), Radiance-based validation of the V5 MODIS land-surface temperature product, *Int. J. Remote Sens.*, *29*(17–18), 5373–5395, doi:10.1080/01431160802036565.

Wan, Z. M., Y. L. Zhang, Q. C. Zhang, and Z. L. Li (2002), Validation of the land-surface temperature products retrieved from Terra Moderate Resolution Imaging Spectroradiometer data, *Remote Sens. Environ.*, *83*(1–2), 163–180, doi:10.1016/S0034-4257(02)00093-7.

Wang, A., M. Barlage, X. Zeng, and C. S. Draper (2014), Comparison of land skin temperature from a land model, remote sensing, and in situ measurement, *J. Geophys. Res. Atmos.*, *119*, 3093–3106, doi:10.1002/2013JD021026.

Wang, C., and D. B. Enfield (2001), The tropical Western Hemisphere warm pool, *Geophys. Res. Lett.*, *28*, 1635–1638, doi:10.1029/2000GL011763.

Wang, K. (2014), Sampling biases in datasets of historical mean air temperature over land, *Sci. Rep.*, *4*, 4637, doi:10.1038/srep04637.

Wang, K., and R. E. Dickinson (2012), A review of global terrestrial evapotranspiration: Observation, modeling, climatology, and climatic variability, *Rev. Geophys.*, *50*, RG2005, doi:10.1029/2011RG000373.

Wang, K., and R. E. Dickinson (2013), Global atmospheric downward longwave radiation at the surface from ground-based observations, satellite retrievals, and reanalyses, *Rev. Geophys.*, *51*, 150–185, doi:10.1002/rog.20009.

Wang, K., and S. Liang (2009), Evaluation of ASTER and MODIS land surface temperature and emissivity products using long-term surface longwave radiation observations at SURFRAD sites, *Remote Sens. Environ.*, *113*(7), 1556–1565.

Wang, K., and C. Zhou (2015), Regional contrasts of the warming rate over land significantly depend on the calculation methods of mean air temperature, *Sci. Rep.*, *5*, 12,324, doi:10.1038/srep12324.

Wang, K., Z. Wan, P. Wang, M. Sparrow, J. Liu, X. Zhou, and S. Haginoya (2005), Estimation of surface long wave radiation and broadband emissivity using Moderate Resolution Imaging Spectroradiometer (MODIS) land surface temperature/emissivity products, *J. Geophys. Res.*, *110*, D11109, doi:10.1029/2004JD005566.

Wang, K. C., Z. Wan, P. Wang, M. Sparrow, J. Liu, and S. Haginoya (2007), Evaluation and improvement of the MODIS land surface temperature/emissivity products using ground-based measurements at a semi-desert site on the western Tibetan Plateau, *Int. J. Remote Sens.*, *28*(11), 2549–2565.

Zeng, X., Z. Wang, and A. Wang (2012), Surface skin temperature and the interplay between sensible and ground heat fluxes over arid regions, *J. Hydrometeorol.*, *13*(4), 1359–1370, doi:10.1175/JHM-D-11-0117.1.

Zhou, C., and K. Wang (2016a), Biological and environmental controls on evaporative fractions at AmeriFlux sites, *J. Appl. Meteorol. Climatol.*, *55*(1), 145–161, doi:10.1175/JAMC-D-15-0126.1.

Zhou, C., and K. Wang (2016b), Coldest temperature extreme monotonically increased and hottest extreme oscillated over Northern Hemisphere land during last 114 years, *Sci. Rep.*, *6*, 25,721, doi:10.1038/srep25721.

Zhou, C., and K. Wang (2016c), Evaluation of surface fluxes in ERA-Interim using flux tower data, *J. Clim.*, *29*(4), 1573–1582, doi:10.1175/JCLI-D-15-0523.1.

Zhou, C., and K. Wang (2016d), Spatiotemporal divergence of the warming hiatus over land based on different definitions of mean temperature, *Sci. Rep.*, *6*, 31,789, doi:10.1038/srep31789.

Zhou, L., R. E. Dickinson, Y. Tian, M. Jin, K. Ogawa, H. Yu, and T. Schmugge (2003), A sensitivity study of climate and energy balance simulations with use of satellite-derived emissivity data over Northern Africa and the Arabian Peninsula, *J. Geophys. Res.*, *108*(D24), 4795, doi:10.1029/2003JD004083.

Zhou, L., R. E. Dickinson, Y. Tian, R. S. Vose, and Y. Dai (2007), Impact of vegetation removal and soil aridation on diurnal temperature range in a semiarid region: Application to the Sahel, *Proc. Natl. Acad. Sci. U.S.A.*, *104*(46), 17,937–17,942, doi:10.1073/pnas.0700290104.

Zhou, L., A. Dai, Y. Dai, R. Vose, C.-Z. Zou, Y. Tian, and H. Chen (2009), Spatial dependence of diurnal temperature range trends on precipitation from 1950 to 2004, *Clim. Dyn.*, *32*(2–3), 429–440, doi:10.1007/s00382-008-0387-5.

Zhou, L., R. Dickinson, A. Dai, and P. Dirmeyer (2010), Detection and attribution of anthropogenic forcing to diurnal temperature range changes from 1950 to 1999: Comparing multi-model simulations with observations, *Clim. Dyn.*, *35*(7–8), 1289–1307, doi:10.1007/s00382-009-0644-2.

Zhou, L., H. Chen, and Y. Dai (2015), Stronger warming amplification over drier ecoregions observed since 1979, *Environ. Res. Lett.*, *10*(6), 064012, doi:10.1088/1748-9326/10/6/064012.

Zhuo, H., Y. Liu, and J. Jin (2016), Improvement of land surface temperature simulation over the Tibetan Plateau and the associated impact on circulation in East Asia, *Atmos. Sci. Lett.*, *17*(2), 162–168, doi:10.1002/asl.638.